J Mater Sci: Mater Electron (2023) 34:135

A detailed research for determination of Er/Gd co-doping effect in ZnO-NPs thin films on optical, electrical and crystallographic properties

E. Asikuzun Tokeser[1,*], O. Ozturk[2], S. Kurnaz[3], C. Cicek[2], and T. Seydioglu[4]

[1] *Department of Metallurgical and Materials Engineering, Faculty of Engineering and Architecture, Kastamonu University, 37100 Kastamonu, Turkey*
[2] *Department of Electrical and Electronics Engineering, Faculty of Engineering and Architecture, Kastamonu University, Kastamonu, Turkey*
[3] *Research and Application Center, Kastamonu University, Kastamonu, Turkey*
[4] *Department of Electronics and Automation, Kastamonu Vocational School, Kastamonu University, Kastamonu, Turkey*

Received: 13 September 2022
Accepted: 10 November 2022
Published online: 17 January 2023

ABSTRACT

Undoped, Er- and Gd-doped ZnO transparent semiconductor thin films were coated on non-alkaline glass using the sol–gel dip coating method. Methanol and ethanolamine (MEA) were chosen as solvents and stabilizers. Er doping concentration was maintained at 5%. The effects of both different dopants and different dip numbers on the optical, electrical and structural properties of ZnO thin films were analyzed. According to the XRD patterns, hexagonal structure was seen in all films. The optical transmittance of impurity elements-doped ZnO thin films increased with the increasing of Gd doping. High transparency was determined to doped films in the visible region. The electrical properties of the Er/Gd co-doped ZnO thin films were measured by Van der Pauw Hall measurements technique that determined the bulk carrier concentration, the Hall mobility and the resistivity at room temperature. Er- and Gd-doped films show lower Hall mobility and resistivity than undoped ZnO thin films. In the bulk carrier concentration, it was seen that there was an increase in 5 dips and 10 dips, while it decreased in 20 dips.

1 Introduction

Dilute magnetic semiconductors (DMS) are attracting a lot of attention due to their potential applications in spintronic devices such as ultrafast optical switches, optical insulators, logic devices, non-volatile memory, light-emitting diodes and transistors [1–4]. II–VI and III–V transition metal-doped semiconductors are widely studied in DMSs. One of the most interesting materials is ZnO, which has a wide direct band gap

Address correspondence to E-mail: easikuzun@kastamonu.edu.tr

https://doi.org/10.1007/s10854-022-09585-9

of 3.2 eV, a large exciton binding energy of 60 meV and a wurtzite phase. It is also an *n*-type oxide semiconductor material with a wide resistivity range (10^{-4}–10^{12} Ω cm), high transparency and Hall mobility (200 cm^2/Vs). ZnO is a wide bandgap and II–VI group compound semiconductor.

ZnO is important for optoelectronic devices because of its non-toxicity, abundance and low price. ZnO-based thin films display high transmittance in the visible region and a wide range of electrical conductivity. ZnO-based transparent conductive oxide (TCO) thin films are used as liquid crystal displays and transparent electrodes in solar cells. In addition, it is suitable for using as a sensor layer in ultraviolet photodetectors and an active layer in thin-film transistors.

In order to achieve a level of conductivity in ZnO films compared to metallic films, it is important to include additives that can replace Zn in the ZnO crystal. III group elements (such as Al, B, In and Ga) and IV group elements (such as Zr, Ti, Hf and Sn) that are the most common dopants acting as donors are utilized to control or/and improve electrical characterization in ZnO thin films [5, 6]. The effect of the doping is connected with the difference between the ionic radius and electronegativity of Zn and dopant element. Doping atoms whose ionic radius is close to Zn^{+2} (0.74 Å) can be easily replaced by Zn^{+2} and thus cause smaller lattice defect.

Sol–gel process, which is used in this study, facilitates the low cost preparation of large-area thin films. In addition, this method ensures easy control over film thickness and composition. However, thickness of oxide film may be controlled with coating conditions and regulations to viscosity of solution [7–9].

The production of triple-structured $Zn_{1-x}Er_{0.05}Gd_xO$ thin films at different coating thicknesses and examining its effects on the structure will be an important contribution to the literature. For this purpose, the data we obtained from this study were explained in detail in the following sections.

2 Materials and methods

In the preparation of the solution, 99.9% purity $Zn(CH_3CO_2)_2.2H_2O$ (zinc acetate dihydrate), $Gd(OOCCH_3)_3.xH_2O$ (gadolinium III acetate-hydrate-99.9% purity) and $C_{15}H_{21}ErO_6$ (erbium III 2,4-pentanedione-99.9% purity) powder compounds were used. According to the $Zn_{1-x}Er_{0.05}Gd_xO$ compound, the doping values of x were determined as 0.01, 0.02, 0.03, 0.04, 0.05. $Zn(CH_3CO_2)_2.2H_2O$, $C_{15}H_{21}ErO_6$ and Gd_2O_3 powders were weighed in appropriate stoichiometric ratios using precision balances. 50 ml methanol and 0.6 ml methanolamine were used. The prepared solutions were stirred for 8 h in a heated magnetic stirrer. The cleaned microscope glasses were immersed vertically in the prepared solution slowly and withdrawn at the same speed without being kept in the solution. The vertical furnace temperature in the mechanism was set to 350 °C. With this process, Gd-doped thin films coated as 5, 10 and 20 dips were obtained. Finally, the coated samples were prepared for 30 min at 600 °C using a muffle furnace. The nano-thin film samples were named as undoped ZnO, Gd001, Gd002, Gd003, Gd004 and Gd005.

In this study, the D8 Advance Bruker diffractometer (XRD) (using Cu-K_α radiation λ = 0.154 nm in the range of $3° \leq 2\theta \leq 90°$), ICDD PDF2-2002 data cards and the Bruker-EVA 10.0.1.0 analysis program were used for lattice parameters and phase structure. In addition, the Ecopia brand HMS-5500 Hall effect measurement system and the SHIMADZU brand UV–VIS spectrophotometer (in the range of 190–1100 nm wavelength) were used for electrical and optical analyses, respectively.

3 Results and discussions

3.1 XRD measurements

The structural properties of the thin films were measured by XRD spectra. Typical XRD patterns of all samples (thin films) were given in Fig. 1. All patterns belong to the peaks of ZnO. These peaks were compatible with one of the data of JCPDS card no: 01-080-0074 of hexagonal wurtzite ZnO [10].

According to XRD analysis, it was seen that all films have wurtzide type structure. As seen in Fig. 1, undoped and Er/Gd co-doped ZnO thin films were oriented along the (002) plane. In Fig. 1a, Gd002 seemed to adhere better to the glass surface than the others, and has the highest intensity at 5 dips. It was seen that the intensity of Gd003 increased at 10 dips (Fig. 1b). In the 20 dips in Fig. 1c, it was seen that the intensity of Gd002 decreased, but Gd001, Gd003 and

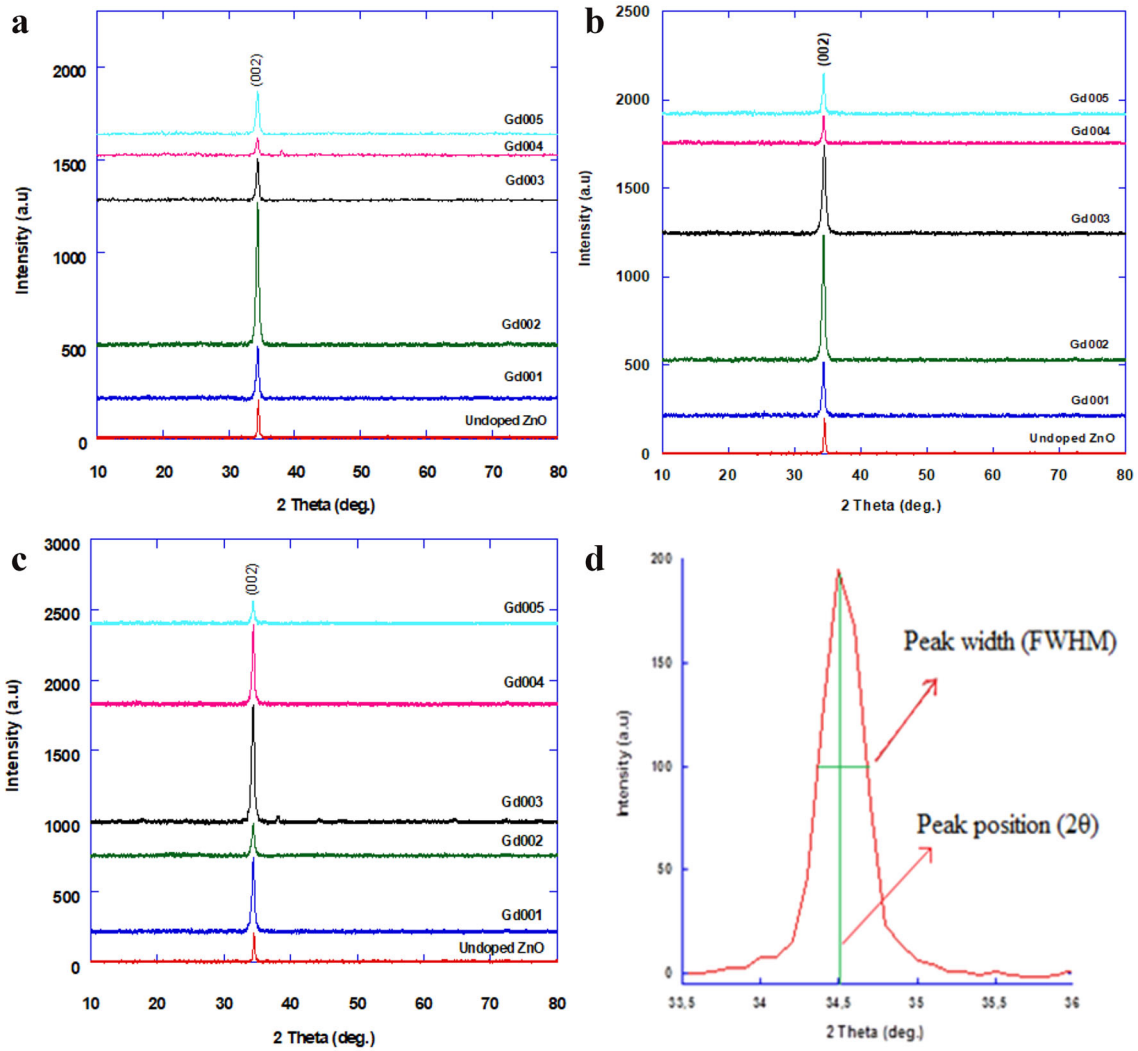

Fig. 1 XRD patterns of **a** 5-dip, **b** 10-dip, **c** 20-dip ZnO-based thin films and **d** the schematic diagram of FWHM

Gd004 increased. The schematic diagram of FWHM is shown in Fig. 1d. FWHM values of doped films were wider than undoped film [11]. In addition, the FWHM values increased with the increase of the coating thickness. The crystallite size (D) of all thin films was calculated with the Debye–Scherrer's formula. As observed in Table 1, the *D* decreased with increasing both the Gd doping and the coating thickness. A larger *D* is an indication of less ordered grains and fewer micro-defects in the grains. It was evident that Gd-doped ZnO thin films have better crystal size than undoped thin films. This size difference may be due to the difference between the ionic radius of doping elements and the zinc. In addition, the incorporation of dopant elements into the ZnO structure may result in the formation of more nucleation centers. Moreover, it was seen that (002) peak values shifted to smaller angles with increasing the Gd doping (Table 1). We say that a/c parameters increased with the contribution of Er/Gd. This is an expected result. The Zn^{+2} (0.88 Å) has smaller ionic radius than Er^{+3} (1.03 Å) and Gd^{+3} (1.07 Å) ions. The larger lattice parameter means that Er^{+3} and Gd^{+3} are included into the lattice of ZnO and replaced by Zn clusters [12, 13].

In addition to the structural analysis comments, the following values were also calculated.

(a) Dislocation density (δ)

The dislocation density is the number of dislocations of a crystal sample in a unit volume or measured by counting the number of dislocation lines that thread a unit area of surface.

Table 1 Grain size and lattice parameters of ZnO-based thin films

Samples	Grain size (nm)			*c* Lattice parameter (Å)		
	5 dips	10 dips	20 dips	5 dips	10 dips	20 dips
Undoped ZnO	28.96	27.15	25.55	5.21	5.21	5.21
Gd001	21.71	19.74	18.48	5.21	5.21	5.21
Gd002	21.71	17.37	18.48	5.21	5.21	5.22
Gd003	22.27	17.03	17.37	5.21	5.22	5.22
Gd004	21.71	18.10	18.88	5.22	5.22	5.22
Gd005	17.37	17.37	18.09	5.22	5.22	5.22

$$\delta = 1/D^2. \quad (1)$$

(b) Lattice strain (ε)

Lattice strain is a measure of the distribution of lattice constants, such as lattice dislocations, which arises from crystal imperfections.

$$\varepsilon = \beta/4\tan\theta. \quad (2)$$

3.1.1 *What causes lattice strain?*

The lattice defects/oxygen vacancies in the structure were formed by loss oxygen and/or electrons. This defect creates to lattice strain in crystals. The factors such as partial oxygen pressure, ions doping, applied electric field, and stress of surface can be produced to defects.

The stress formula for the hexagonal lattice parallel to the thin film surface is as follows.

$$\sigma = \frac{2c_{13}^2 - c_{33}(c_{11} + c_{12})}{2c_{13}} E, \quad (3)$$

Here $E = (c - c_0)/c_0$ and it expresses the strain of film in the *c*-axis perpendicular to the sub-base surface. *c* is the lattice parameter of the thin film and c_0 is the free deformation lattice parameter [8]. The values of c_{11}, c_{33}, c_{12}, c_{13} are the elastic constants of the crystal, and for ZnO deposited on the glass substrate, these expressions take as c_{11} = 208.8 nm, c_{33} = 213.8 nm, c_{12} = 119.7 nm, c_{13} = 104.2 nm and c_0 = 0.5205 nm. When these values were written into the stress formula;

$$\sigma = -233(c - c_0)/c_0(GPa). \quad (4)$$

Calculated lattice strain, dislocation density and stress values are given in Table 2. As can be seen from the table, these values increased with the increase of both the Gd contribution and the coating thickness. The increase in the number of dislocations in the unit volume of the crystal may cause an increase in the lattice defects resulting from these defects and thus an increase in the lattice strain may occur. Accordingly, the increase in *c* lattice parameter can be attributed to this result.

In addition, the negative strain values obtained mean that the films are under compressive strain, as can be noticed from the *c*-axis values, which are slightly smaller than that of the bulk. This compressive strain increased as the Gd doping increases.

3.2 Optical measurements

The transmittance and absorbance spectra of the thin films were determined at room temperature using UV–Vis spectrophotometer. According to the optical transmittance spectra, a sharp absorption was observed in the wavelength range of 350–380 nm at all transitions (Fig. 2). When dopant elements were added to ZnO thin films, no significant shift of the absorption edges was observed. When the number of dips increases, it was observed that the band edges are distorted and the transmittance values decreased (Table 3).

As seen in Table 3, the average optical transmission values for ZnO thin films vary between 72 and 92% for 5 dips in the visible region (400–700 nm). Further, these values ranged from 81%-79% in films coated with 10 dips and 82–72% in films coated with 20 dips. If each coating thickness was compared within itself, it was said that the transparency value increased with increasing the Gd doping. Higher values than the transmittance value of the undoped ZnO sample were obtained. The transmittance of ZnO-based thin films is affected by defects such as film thickness, surface roughness, particle size, and nanopores.

Table 2 Dislocation density, stress and lattice strain parameters of ZnO-based thin films

Samples	Dislocation density ($\times 10^{-3}$) (nm^{-2})			Stress (GPa)			Lattice strain (nm)		
	5 dips	10 dips	20 dips	5 dips	10 dips	20 dips	5 dips	10 dips	20 dips
Undoped ZnO	1.19	1.19	4.215	4.215	4.215	1.19	− 0.349	− 0.349	− 0.349
Gd001	2.12	2.57	5.655	6.196	6.645	2.93	− 0.459	− 0.488	− 0.389
Gd002	2.12	3.31	5.655	7.041	6.645	2.93	− 0.422	− 0.626	− 0.801
Gd003	2.12	3.45	5.655	7.182	6.928	3.18	− 0.538	− 1.056	− 0.890
Gd004	2.12	3.18	5.655	6.900	6.504	2.81	− 0.859	− 0.895	− 0.948
Gd005	3.32	3.31	7.069	7.041	6.786	3.06	− 0.906	− 0.872	− 0.962

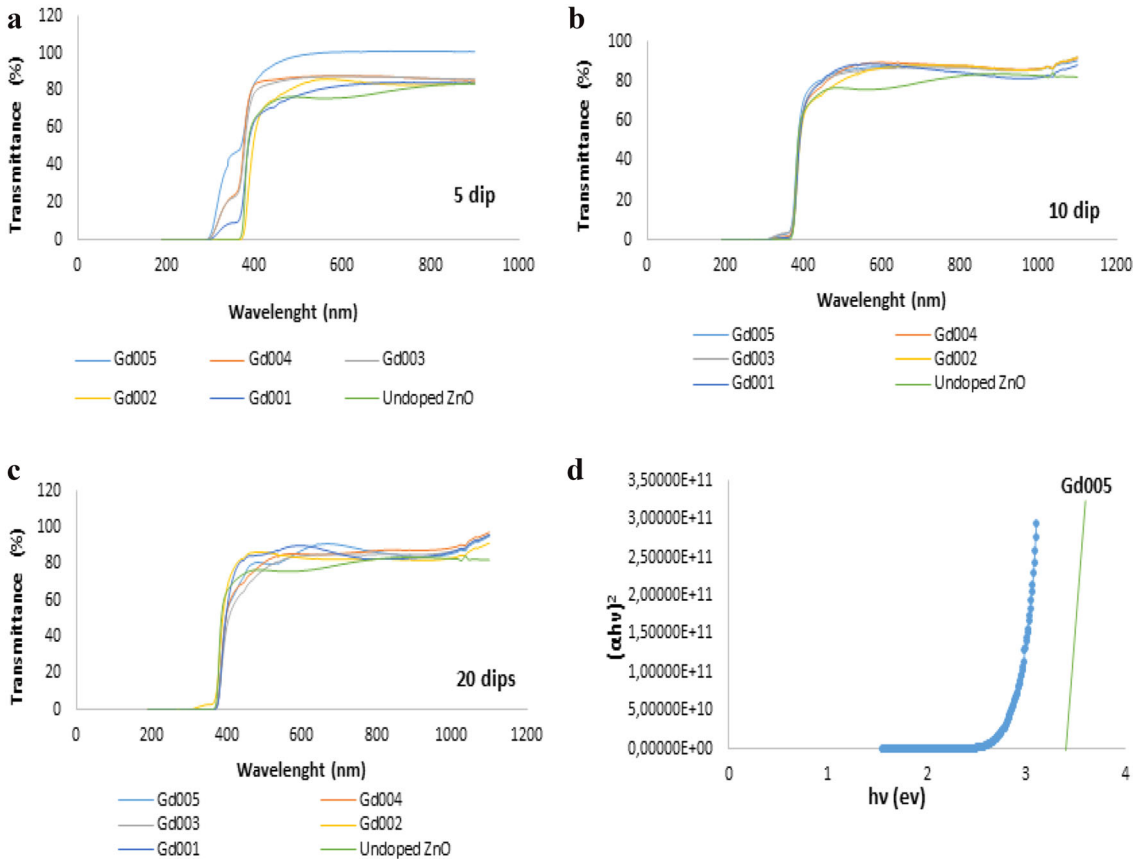

Fig. 2 Optical transmittance spectra of **a** 5-dip, **b** 10-dip, **c** 20-dip ZnO-based thin films and **d** the plots of $(\alpha hv)^2$ vs (hv) for 5-dip coated %5 Gd-doped ZnO-based thin film

Another important value for thin films was the optical band gap. This value can be calculated using the following equation [14, 15].

$$(\alpha hv) = A(hv - E_g)^{1/2}, \quad (5)$$

where α is the absorption coefficient, hv is the photon energy, A is a constant, and E_g is the optical band gap. The optical band gap of the ZnO thin film is evaluated to have a direct optical transition. It is well known that a direct transition is possible across the band gap between the valence and conduction band edges in the k-space [16–18]. During this transition, the total energy and momentum of the electron-photon system must be conserved. Figure 2d shows $(\alpha hv)^2 - hv$ graph of 5-dip coated %5 Gd-doped ZnO-

Table 3 Energy band gap, transmittance and absorbance values for ZnO and Er/Gd co-doped ZnO-based thin films

Samples	Energy band gap (eV)			Transmittance (%)			Absorbance (%)		
	5 dips	10 dips	20 dips	5 dips	10 dips	20 dips	5 dips	10 dips	20 dips
Undoped ZnO	3.10	3.15	3.16	81.18	81.10	82.05	0.090	0.088	0.085
Gd001	3.05	3.00	3.06	73.94	75.95	69.88	0.131	0.119	0.155
Gd002	3.02	2.99	3.05	69.21	75.33	74.32	0.159	0.123	0.128
Gd003	3.03	2.99	3.03	83.14	76.82	65.23	0.080	0.114	0.185
Gd004	3.00	2.99	3.03	85.38	77.27	69.26	0.068	0.111	0.159
Gd005	3.00	2.97	3.03	92.55	79.36	72.10	0.033	0.100	0.142

based thin film. The same graph was drawn for each sample. Energy band gap values are given in Table 3.

For 5 dips, while the E_g was 3.10 eV for undoped film, it was in the range of 3.00–3.05 eV for Gd-doped films. For 10 dips, the E_g of the undoped film was 3.15 eV; it was in the range of 2.97–3.00 eV for the Gd-doped films; for 20 dips, the E_g of the undoped film was 3.16 eV, it ranged from 3.03 eV to 3.06 eV. Obtained E_g values were smaller than for undoped films. The E_g values increased with increasing the number of dips. It decreased with Gd doping. The E_g of ZnO thin film was lower than amorphous ZnO thin films. This E_g narrowing was due to the increase in the band tail width. Semiconductor materials combined with dopants cause the formation of band tails in the E_g.

In addition, we can say that the E_g increased as the nanoparticle size decreases. This situation has been expressed in the literature that ZnO nanoparticles change the optical band gap [19].

$$E_g(\text{nano crystal}) = E_g(\text{bulk}) + \frac{\pi^2\hbar^2}{2D^2}\left(\frac{1}{m_e^*} + \frac{1}{m_h^*}\right), \quad (6)$$

Here m_e^* and m_h^* are the effective masses of electrons and holes. D is the crystallite size obtained from the Scherrer equation, E_g (nanocrystal) is the optical band gap of ZnO nanocrystalline and E_g (bulk) is the optical band gap of bulk ZnO. The E_g of bulk ZnO is 3.3 eV. The effective masses of electrons and holes of ZnO are $0.24m_o$ and $0.45m_o$, respectively [20]. This value was obtained in the range of 3.317–3.349 eV with increasing Gd doping for 5 dips (Table 4). The E_g increased with decreasing the crystallite size. The same behavior was observed for 10- and 20-dip-coated films.

In addition, the Urbach energy can be calculated using the following equation.

$$\alpha = \alpha_0 \exp\left[\frac{h\vartheta - E_I}{E_u}\right], \quad (7)$$

Here E_I and α_0 are constants and E_u is the Urbach energy, which expresses the width of the exponential absorption edge [21–24]. The Urbach energy is related to the optical transmittance between the valence band and the conduction band. Figure 3 shows variation of the photon energy versus $In\alpha$ of all thin films. The slope of the graph gives the value of $1/E_u$. Calculated E_u values are given in Table 4. E_u values decreased with increasing the coating thickness and number of dips. With the Gd doping, E_u value was higher than undoped ZnO. The variation of E_u values is affected by all possible defects such as structural disorder and carrier impurity interactions. In addition, this result may be due to the dependence of the photon energy and the optical absorption coefficient and the trap levels at grain boundaries. The density of these states exponentially decreased with energy, which is consistent with Tauc theory [25]. If Eq. 7 is rewritten;

$$\alpha = \alpha_0 exp\left[\frac{\beta}{kT}(E - E_I)\right], \quad (8)$$

Here β is the steepness parameter. It expresses the broadening of the absorption edge due to electron–phonon or exciton-phonon interaction. If the edge width (E_u) is related to the slope of Eq. 8, β is found as $\beta = kT/E_u$. The β value was calculated by taking T = 300 K and was given in Table 4.

ZnO absorbs UV light by band-to-band transition. Because of this feature, it can be used as a transparent electrode in flat panel displays and solar cells, anti-reflective coatings, optical filters and optoelectronic devices. And also it is used as a semiconductor gas sensor because its conductivity changes when exposed to oxidizing gases such as ozone.

Table 4 Urbach energy, steepness parameter and E_g (nanocrystal) as a function of Gd content

Samples	Urbach energy (eV)			Steepness parameter (β)			E_g (nanocrystal) (eV)		
	5 dips	10 dips	20 dips	5 dips	10 dips	20 dips	5 dips	10 dips	20 dips
Undoped ZnO	149.05	147.01	145.60	0.173	0.175	0.177	3.317	3.320	3.322
Gd001	127.99	138.95	126.22	0.201	0.186	0.204	3.331	3.338	3.343
Gd002	127.79	146.50	148.11	0.202	0.176	0.174	3.331	3.349	3.343
Gd003	188.61	153.01	151.77	0.137	0.168	0.170	3.330	3.351	3.349
Gd004	178.56	152.77	139.70	0.144	0.169	0.185	3.331	3.345	3.342
Gd005	190.58	150.87	138.00	0.135	0.171	0.187	3.349	3.349	3.345

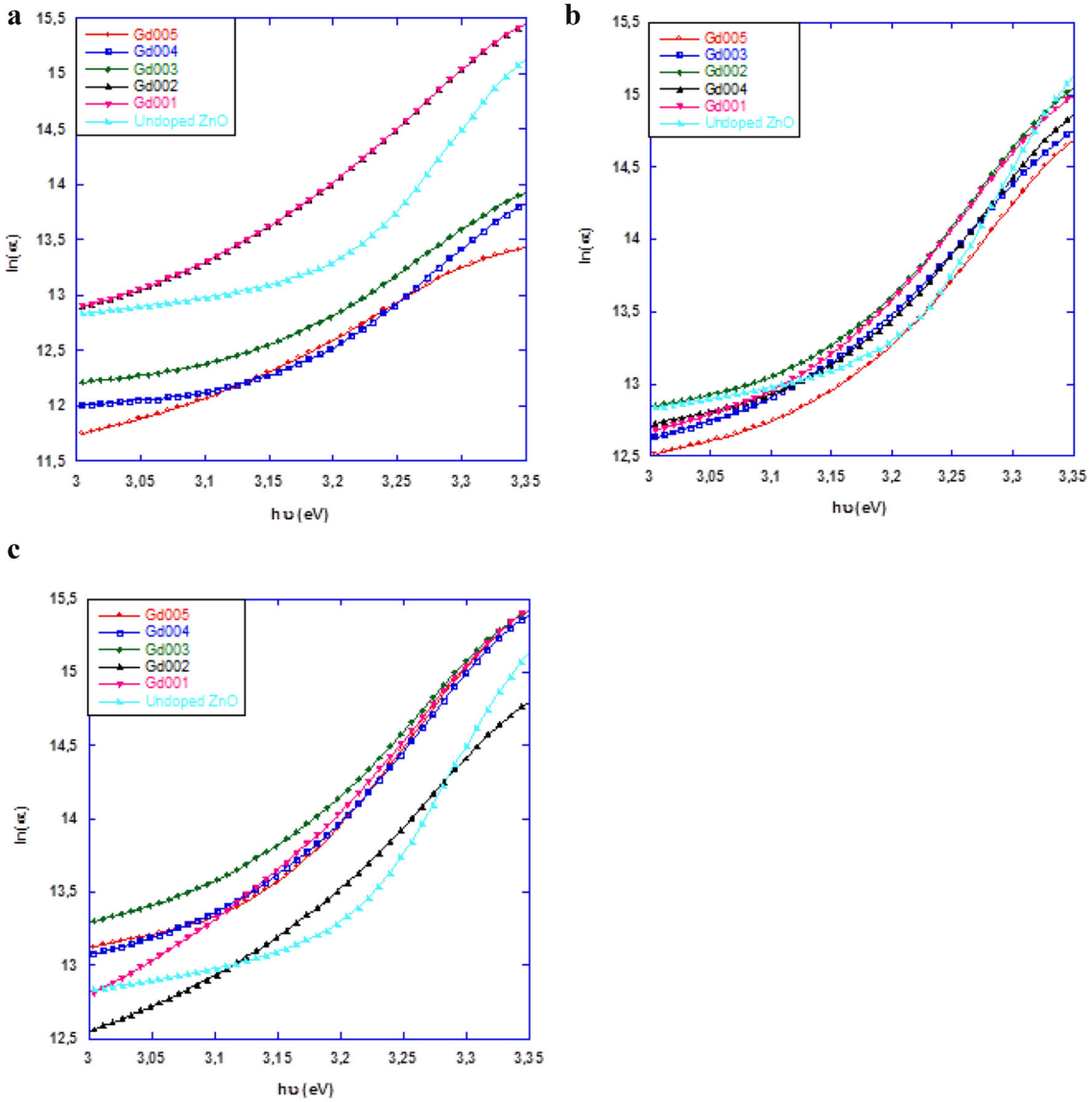

Fig. 3 The plots of Inα vs ($h\nu$) of **a** 5-dip, **b** 10-dip, **c** 20-dip ZnO-based thin films

3.3 Electrical measurements

The electrical effects of both different dips and Er/Gd substitution were analyzed using Van der Pauw Hall system [26–28]. At room temperature, Fig. 4 shows the alteration of bulk resistivity, mobility and carrier concentration of Gd-doped samples (0 − 5% doping rate).

As illustrated in Table 5, with Gd concentration increasing from 0% to 5%, the resistivity of the films increased from 8.56 to 12.50 Ω·cm for 5 dips. For 10 dips and 20 dips, these values increased from 10.53 to 12.70 Ω·cm and 15.22 to 13.50 Ω·cm, respectively. The resistivity of films is affected from surface and point defects, lattice and impurity scattering and number of free carriers.

The carrier concentration initially increased rapidly up to 10-dip coating, thereafter decreased slowly for 20 dips (Table 5). Similarly, the carrier concentration increased up to 10 dips with an increasing the Gd concentration. And then decreased in the 20 dips coated. The increment of carrier concentration can be because of the inclusion of Gd ions interstitial positions or replacement of Gd^{+3} ions at Zn^{+2} cation sites [29–32]. The reduction of the carrier concentration at 20 dips is due to the increment in grain boundary defects. These defects are traps for free carriers.

It was further seen from Fig. 4 that the Hall mobility of the films decreased quickly from 0.732 $cm^2/V{\cdot}s$ for undoped ZnO to 0.119 $cm^2/V{\cdot}s$ for 5% Gd content, and also increased to 20 dips from 5 dips. For higher Gd concentrations, the Hall mobility was saturated for all films. Firstly, Hall mobility

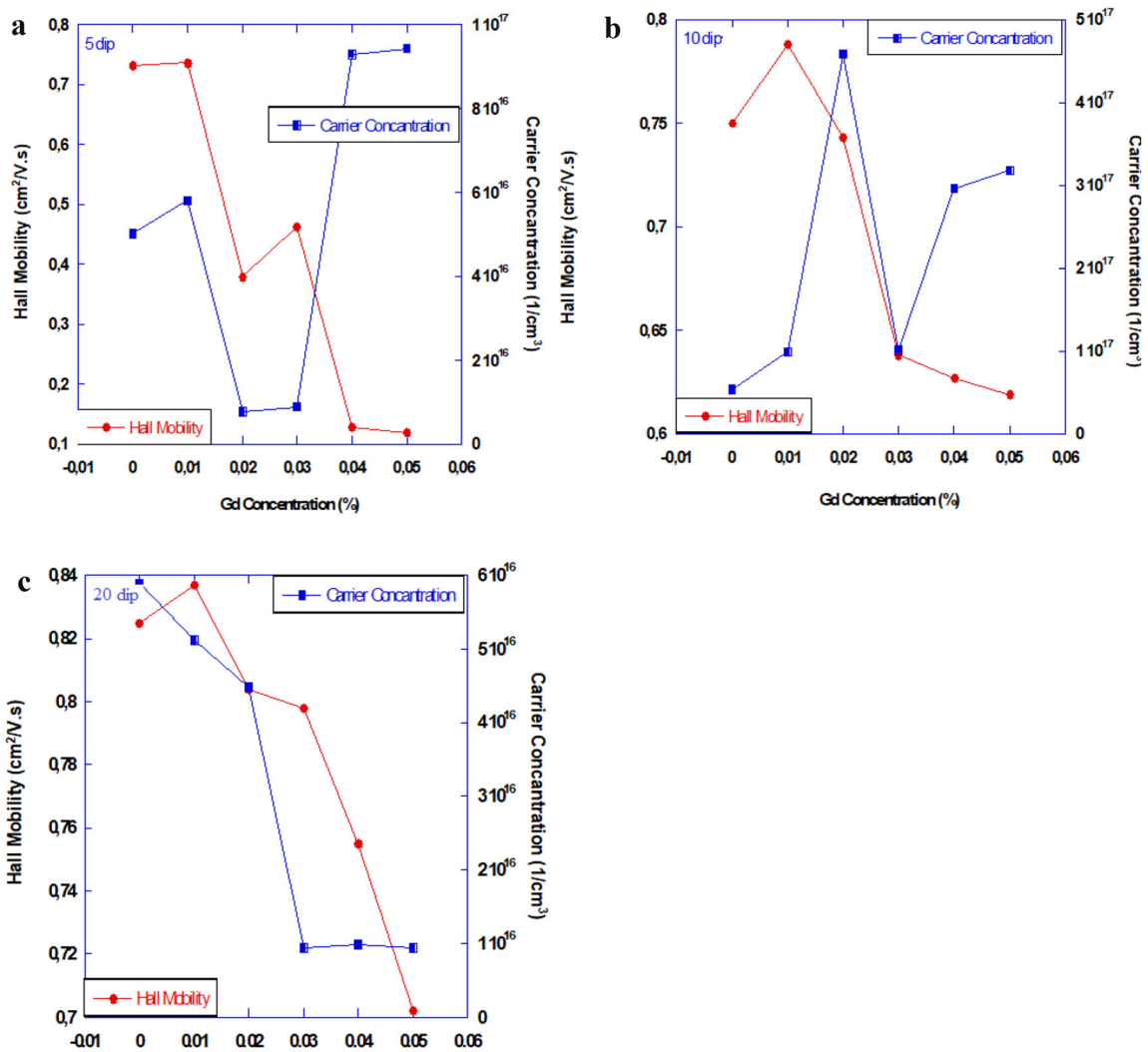

Fig. 4 Hall mobility and carrier concentration of **a** 5-dip, **b** 10-dip, **c** 20-dip ZnO-based thin films

Table 5 Variations of resistivity and bulk carrier concentration values of for ZnO and Er/Gd co-doped ZnO thin films

Samples	Resistivity (Ω·cm)			Carrier concentration ($\times 10^{16}$/cm^3)		
	5 dips	10 dips	20 dips	5 dips	10 dips	20 dips
Undoped ZnO	8.56	10.53	15.22	5.01	5.32	5.89
Gd001	8.27	7.36	14.90	5.81	9.89	5.12
Gd002	8.31	8.72	12.20	7.60	45.8	4.48
Gd003	10.60	11.60	12.50	8.87	10.1	9.32
Gd004	12.40	12.00	12.20	9.29	29.6	9.88
Gd005	12.50	12.70	13.50	9.43	31.8	9.39

decreased. It can be explained that ionized impurities were scattered with conduction electrons because of Gd doping. The carrier mobility is controlled essentially by the scattering of the charge carriers. In the low temperature region, the ionized impurity scattering is an important factor for the degenerate semiconductors. The changing of Hall mobility of Gd-doped films was summarized in Table 6. The results were compatible with grain size. The number of grain boundaries increased with decreasing grain sizes or vice versa. For 5 dips and 10 dips, the scattering centers and the increment in carrier concentration recompense one other in stable mobility and resistivity.

4 Conclusions

In this work, Er/Gd co-doped ZnO thin films have been prepared by the sol–gel dip coating method using $Zn(CH_3CO_2)_2.2H_2O$, $C_{15}H_{21}ErO_6$ and Gd_2O_3 as precursors. The effect of Gd doping (0–5%) and number of dip coating on the optical, structural and electrical properties of Er/Gd co-doped ZnO thin films has been investigated. The XRD pattern of thin films was shown wurtzide type structure. XRD results were shown that the crystallinities were much deteriorated with increasing Gd content. This is due to difference between ionic radius of Zn^{+2}, Er^{+3} and Gd^{+3} which affects grain size, lattice parameter, dislocation density, stress and lattice strain. The *D* decreased with increasing both the Gd doping and the coating thickness. From the UV–Vis spectroscopy measurements were seen that the maximum transmittance of all thin films was at visible region and decreased to the ultraviolet region. The optical band gap, transmittance, absorbance, Urbach energy, Steepness parameter values of ZnO thin film were determined. The optical direct band gap of undoped ZnO thin films prepared by 5 dips, 10 dips and 20 dips were 3.10 eV, 3.15 eV and 3.16 eV, respectively. With increased Gd content, the optical direct band gap decreased to 3.00 eV, 2.97 eV and 3.03 eV, respectively. Obtained Eg values were smaller than for undoped films. The Eg values increased with increasing the number of dips. It decreased with Gd doping. The Eg of ZnO thin film was lower than amorphous ZnO thin films. The electrical properties of the Er/Gd co-doped ZnO thin films were measured by Van der Pauw Hall measurements technique that determined the bulk carrier concentration, the Hall mobility and the resistivity at room temperature. With increased Gd doping and number of dips, it was seen that the Hall mobility decreased and the resistivity increased. In the bulk carrier concentration, it was seen that there was an increase in 5 dips and 10 dips, while it decreased in 20 dips. Considering all these results, all thin films excepted Gd002 in 5 dips have the highest transmittance which results in the best ZnO-based transparent conductive oxide properties.

Table 6 Variations of Hall mobility values of for ZnO and Er/Gd co-doped ZnO nano thin films

Samples	Hall mobility (cm^2/V·s)		
	5 dips	10 dips	20 dips
Undoped ZnO	0.732	0.750	0.825
Gd001	0.736	0.788	0.837
Gd002	0.379	0.743	0.804
Gd003	0.462	0.638	0.798
Gd004	0.127	0.627	0.755
Gd005	0.119	0.619	0.702

Author contributions

All authors have contributed sufficiently in the planning, execution, or analysis of this study to be included as authors. All authors have read and agreed to the published version of the manuscript.

Funding

This work was supported by Kastamonu University Scientific Research Projects Coordination Department under the Grant No. KÜ-BAP01/2020-75, KÜ-BAP01/2019-64, KÜ-BAP01/2018-19 and Kastamonu University Research and Application Center for the supports.

Data availability

The data sharing is not applicable to this article because no datasets were generated or analyzed during the current study.

Declarations

Conflict of interest The authors declare that there are no conflicts of interest regarding the publication of this article.

Ethical approval This material is the authors' own original work, which has not been previously published elsewhere. The paper reflects the authors' own research and analysis in a truthful and complete manner. The results are appropriately placed in the context of prior and existing research. All authors have been personally and actively involved in substantial work leading to the paper and will take public responsibility for its content.

References

1. E. Asikuzun, O. Ozturk, L. Arda, D. Akcan, S.D. Senol, C. Terzioglu, Preparation, structural and micromechanical properties of (Al/Mg) co-doped ZnO nanoparticles by sol–gel process. J. Mat. Sci.: Elect. **26**, 8147–8159 (2015)
2. Y. Caglar, M. Caglar, S. Ilican, Microstructural, optical and electrical studies on sol gel derived ZnO and ZnO: Al films. Curr. App. Phys. **12**, 963–968 (2012)
3. Z. Fan, J.G. Lu, Zinc oxide nanostructures: synthesis and properties. J. Nanosci. Nanotech. **5**, 1561–1573 (2005)
4. J.L. Snoek, Non-metallic magnetic material for high frequencie. Philips Techn. Rev. **8**, 353–360 (1946)
5. E. Asikuzun, O. Ozturk, L. Arda, C. Terzioglu, Growth and characterization of nonvacuum Cu doped ZnO thin films. J. Mol. Struct. **1165**, 1–7 (2018)
6. X. Chang, X. Li, Q. Xue, Sensing mechanism of acetone adsorption on charged ZnO and ZnSe surfaces: insights from DFT calculations. Mater. Today Commun. **31**, 103238 (2022)
7. M.A.-A. Salih, M.H. Shinen, Q.S. Kareem, Study of the effect of annealing temperature on the response of nano-films of ZnO to ammonia gas sensor. J. Phys.: Conf. Series **1854**, 012008 (2021)
8. E.R. López-Mena, S.J. Jiménez-Sandoval, O. Jiménez-Sandoval, Samarium-doped ZnO thin films synthesized by sol–gel: structural, optical and electrical properties. Mater. Sci. Semicon. Proces. **126**, 105648 (2021)
9. N. Demirbilek, F. Yakuphanoğlu, M. Kaya, Structural and optical properties of pure ZnO and Al/Cu co-doped ZnO semiconductor thin films and electrical characterization of photodiodes. Materialpruefung/Mater. Test. **63**, 279–285 (2021)
10. Powder Diffraction File 36-1451 for hexagonal Zinc Oxide (1997 JCPDS-International center for Diffraction data)
11. B.D. Cullity, S.R. Stock, *Elements of X-ray diffraction*, 3rd edn. (Prentice Hall, Upper Saddle River, 2001)
12. B. Ayadi, L. ElMir, S. Alaya, K. Djessas, E. Hernandez, Effect of doping concentration on transparency and conductivity of ZnO: Al thin films. Nanotechnology **18**, 445072–445706 (2007)
13. T. Man, C. Hu, H. Lu, Y. Chen, Y. Lin, H. Dong, Effect of annealing temperature on microstructure and hardness of Ni–Co alloy coating. Mater. Today Commun. **31**, 103244 (2022)
14. K.L. Foo, M. Kashif, U. Hashim, W.-W. Liu, Effect of different solvents on the structural and optical properties of zinc oxide thin films for optoelectronic applications. Ceram. Int. **40**, 753 (2014)
15. F. Urbach, The long-wavelength edge of photographic sensitivity and of the electronic absorption of solids. Phys. Rev. **92**, 1324 (1953)
16. J. George, K.S. Joseph, B. Pradeep, T.I. Palson, Reactively evaporated films of indium sulphide. Phys. Status Solid. **106**, 123 (1988)
17. B. Sankara Reddy, B. Sreenivasulu, N. Koteeswara Reddy, S. Venkatramana Reddy, P. Bharath Kumar, Single and bivalent metal-cations co-doped ZnO nanopowders: synthesis and characterization. J. Mat. Sci.: Elect. **33**, 17462–17468 (2022)
18. S.Y. Marzouk, M.A. Azooz, H.M. Elsaghier, N.A. Zidan, W. Abbas, Structural and optical properties of barium titanium

borate glasses doped with ytterbium. J. Mat. Sci.: Elect. **33**, 18054–18071 (2022)
19. M. Caglar, S. Ilican, Y. Caglar, F. Yakuphanoglu, Electrical conductivity and optical properties of ZnO nanostructured thin film. App. Sur. Sci. **255**, 4491–4496 (2009)
20. E.M. Wong, P.C. Searson, ZnO quantum particle thin films fabricated by electrophoretic deposition. Appl. Phys. Lett. **74**, 2939 (1999)
21. H. Yano, J. Sugiyama, A.N. Nakagaito, M. Nogi, T. Matsuura, M. Hikita, K. Handa, Optically transparent composites reinforced with networks of bacterial nanofibers. Adv. Mater. **17**, 153 (2005)
22. R.J. Nussbaumer, W.R. Caseri, P. Smith, T. Tervoort, Polymer-TiO_2 nanocomposites: a route towards visually transparent broadband UV filters and high refractive index materials. Macromol. Mater. Eng. **288**, 44 (2003)
23. V. Srikant, D.R. Clarke, On the optical band gap of zinc oxide. J. Appl. Phys. **83**, 5447 (1998)
24. M. Berber, V. Bulto, R. Kliß, H. Hahn, Transparent nanocrystalline ZnO films prepared by spin coating. Scripta Mater. **53**, 547 (2005)
25. J. Tauc, *Amorphous and liquid semiconductors* (Plenum Press, New York, 1974)
26. S.D. Senol, A. Senol, O. Ozturk, M. Erdem, Effect of annealing time on the structural, optical and electrical characteristics of DC sputtered ITO thin films. J. Mater. Sci. **25**, 4992–4999 (2014)
27. C.Y. Tsay, W.T. Hsu, Sol–gel derived undoped and boron-doped ZnO semiconductor thin films: preparation and characterization. Ceram. Int. **39**, 7425–7432 (2013)
28. L.J. Van der Pauw, A method of measuring the resistivity and Hall coefficient on lamellae of arbitrary shape. Philips Tech. Rev. **20**, 220–224 (1958)
29. I. Winer, G.E. Shter, M. Mann-Lahav, G.S. Grader, Effect of solvents and stabilizers on sol–gel deposition of Ga-doped zinc oxide TCO films. J. Mater. Res. **26**, 1309–1315 (2011)
30. F. Kabir, A. Murtaza, A. Saeed, A. Ghani, A. Ali, S. Khan, K. Li, Q. Zhao, K. Kang Yao, Y. Zhang, S. Yang, Room temperature ferromagnetism in dilute magnetic semiconducting ZnO nanoparticles co-doped with Tb and Fe. J. Mat. Sci.: Elect. **48**, 19606–19617 (2022)
31. P. Velusamy, R. Ramesh Babu, K.T. Aparna, Effect of Sm doping on the physical properties of ZnO thin films deposited by spray pyrolysis technique. AIP Conf. Proc. **1832**, 080085 (2017)
32. P. Velusamy, R. Ramesh Babu, K. Ramamurthi, J. Viegas, E. Elangovan, Structural, microstructural, optical and electrical properties of spray deposited rare-earth metal (Sm) ions doped CdO thin films. J. Mat. Sci.: Elect. **26**, 4152–4164 (2015)